The Astrophysical Journal Letters, 723:L195–L200, 2010 November 10 doi:10.1088/2041-8205/723/2/L195

GAMMA-RAY SIGNAL FROM EARTH-MASS DARK MATTER MICROHALOS

Tomoaki Ishiyama[1], Junichiro Makino[1], and Toshikazu Ebisuzaki[2]
[1] National Astronomical Observatory, Mitaka, Tokyo 181-8588, Japan; ishiyama@cfca.jp, makino@cfca.jp
[2] RIKEN, 2-1, Hirosawa, Wako, Saitama 351-0198, Japan; ebisu@postman.riken.jp
Received 2010 June 17; accepted 2010 September 28; published 2010 October 18

ABSTRACT

Earth-mass dark matter microhalos with a size of ∼100 AU are the first structures formed in the universe, if the dark matter of the universe is made of neutralinos. Here, we report the results of ultra-high-resolution simulations of the formation and evolution of these microhalos. We found that microhalos have the central density cusps of the form $\rho \propto r^{-1.5}$, much steeper than the cusps of larger dark halos. The central regions of these microhalos survive the encounters with stars except in the very inner region of the galaxy down to the radius of a few hundreds parsecs from the galactic center. The annihilation signals from the nearest microhalos are observed as gamma-ray point sources (radius less than 1′), with unusually large proper motions of ∼0.2 deg yr^{-1}. Their surface brightnesses are ∼10% of that of the galactic center. Their signal-to-noise ratios might be better if they are far from the galactic plane. Luminosities of subhalos are determined only by their mass, and they are more than one order of magnitude more luminous than the estimation by Springel et al.: a boost factor can be larger than 1000. Perturbations to the millisecond pulsars by gravitational attractions of nearby Earth-mass microhalos can be detected by the observations of Parkes Pulsar Timing Array.

Key words: cosmology: theory – dark matter – Galaxy: structure – methods: numerical

1. INTRODUCTION

In our universe, dark matter halos evolve in the hierarchical fashion. The smallest microhalos form first, and they merge with each other to form larger halos. The size of the smallest microhalos is determined by the scale of collisional damping and free streaming of dark matter particles. Analytical studies (Zybin et al. 1999; Hofmann et al. 2001; Berezinsky et al. 2003, 2008; Green et al. 2004; Loeb & Zaldarriaga 2005) predicted their mass to be 3.5×10^{-9} to $8.4\times10^{-6}\ M_\odot$, though uncertainty in the theory of supersymmetry enlarges the range further.

Early studies (Berezinsky et al. 2003, 2008; Diemand et al. 2005) suggested that a significant fraction of microhalos born in early universe have survived up to present time, and they might be observed as the dominant sources of the annihilation signal. These microhalos could enhance the annihilation signal by a factor of 2–5 (Berezinsky et al. 2003), whose signature might have already been observed as electron and positron excess (PAMELA (Adriani et al. 2009), ATIC (Chang et al. 2008), PPB-BETS (Torii et al. 2008), and *Fermi* (Abdo et al. 2009b)).

Diemand et al. (2005) simulated the formation of microhalos using *N*-body simulations. They argued that the density profiles were well fitted by a single power law, $\rho(r) \propto r^{-\gamma}$, with slope γ in the range of 1.5–2 down to the radius of $\sim10^{-3}$ pc and that most of microhalos will survive against galactic tidal field and encounters with stars.

On the other hand, Springel et al. (2008) argued that the fraction of the mass in subhalos in the solar neighborhood was significantly lower than that averaged over the entire halo. They assumed that the spatial distribution of the microhalos is the same as that of subhalos with mass $10^5\ M_\odot$ and concluded that the microhalos have a negligible impact on detectability. However, it is not clear whether their result for subhalos with a mass $10^5\ M_\odot$ can be used to estimate the distribution of halos of $10^{-6}\ M_\odot$.

Since Earth-mass subhalos contain no substructures by definition, their central structures can be completely different from that of more massive halos which contain many substructures. However, there is no simulation of Earth-mass halos with sufficient resolution to study their central structure so far. Diemand et al. (2005) used a mass resolution of $1.2\times10^{-10}\ M_\odot$, which was too low to determine the central structures of microhalos.

In this Letter, we report the result of cosmological *N*-body simulations with 100 times better mass resolution and 20 times better spatial resolution compared with that used in Diemand et al. (2005).

2. INITIAL CONDITIONS AND NUMERICAL METHOD

We performed two high-resolution cosmological *N*-body simulations. The number of particles is 1024^3. The size of the simulation box is 30 comoving pc with periodic boundary condition. The mass of particles is $9.43\times10^{-13}\ M_\odot$. For the time integration, we used the GreeM code (Ishiyama et al. 2009a, 2009b). We used a leapfrog integrator with shared and adaptive time steps. The step size was determined as $\min(\sqrt{\varepsilon/|\vec{a}_i|}, \varepsilon/|\vec{v}_i|)$ (minimum of these two values for all particles). We simulated them from $z = 500$ to $z = 31$. The (plummer) softening length ε was constant in the comoving coordinate from $z = 500$ to $z = 100$, and constant in the physical coordinate (5×10^{-5} pc) from $z = 100$ to $z = 31$. To generate the initial particle distribution, we used the MPGRAFIC package (Prunet et al. 2008). We considered two models with different initial matter power spectra.

The matter power spectrum in model A includes the sharp cutoff corresponding to dark matter particle with a mass of 100 GeV (Green et al. 2004). The power spectrum of model B is without cutoff. The cosmological parameters adopted are based on the concordance cosmological model (WMAP1 (Spergel et al. 2003), $\Omega_0 = 0.268$, $\Lambda_0 = 0.732$, $h_0 = 0.71$, $\sigma_8 = 0.9$). However, we used $\sigma_8 = 0.8$ to be close to recent observational ones (Spergel et al. 2007; Komatsu et al. 2009). We did not put any thermal velocities in the initial setup of model A to avoid unphysical density fluctuations in small scales (Colín et al. 2008).

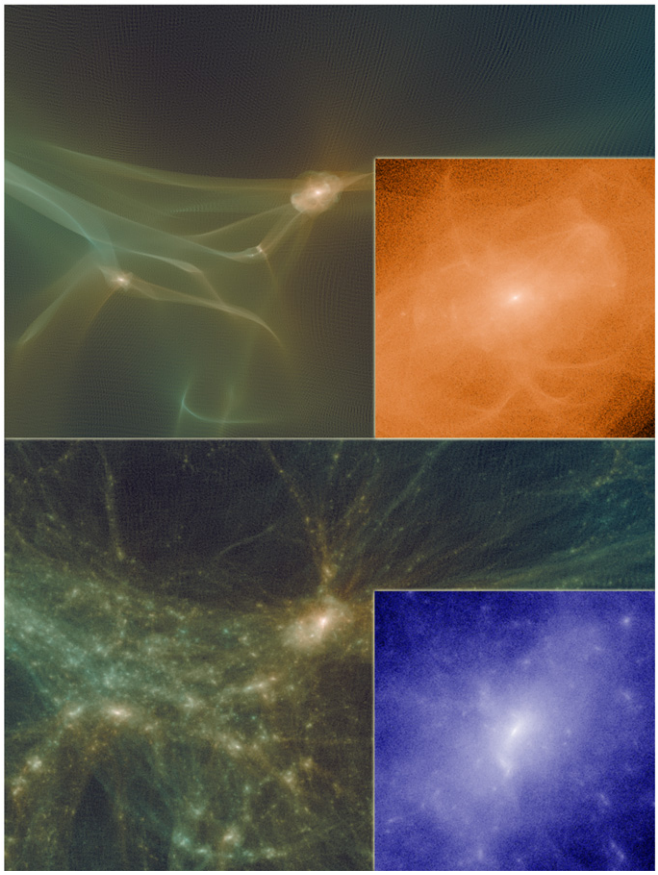

Figure 1. Top and bottom panels show the distribution of dark matter at $z = 31$ for our standard model (A) and model without free-streaming cutoff (B). The width of the images corresponds to 12 comoving pc. Images in the squares are enlargements of single halos. The size of the squares is 0.6 comoving pc (4900 AU in physical units).

Figure 1 shows the snapshots of our simulated universe at $z = 31$. We can see that there are no substructures in one halo of model A, except for caustics generated by nonlinear growth of long-wavelength fluctuations. This structure is quite similar to what we see in warm dark matter simulation (e.g., Bode et al. 2001; Gao & Theuns 2007), and different from that of galaxy-sized or larger dark matter halos (Springel et al. 2008; Ishiyama et al. 2009b; Stadel et al. 2009). The difference comes simply from the initial condition. Our microhalos do not contain smaller fluctuations inside.

3. RESULTS

3.1. Structures of Microhalos

Figure 2 shows the spherically averaged structures of the three most massive halos. We also performed a low-resolution simulation of model A for convergence check (the number of particles was 512^3 and the softening length was 1.0×10^{-4} pc). Two results are identical outside the softening radius. The central density slope for model A is considerably steeper than that for model B. The result of model B is similar to that of large-scale cosmological simulations (Navarro et al. 1996, 2010; Fukushige & Makino 1997; Moore et al. 1999; Fukushige et al. 2004; Stadel et al. 2009). The result of model A is consistent with being a single power law of $\rho \propto r^{-1.5}$, for quite a wide range in the radius. Our result is reliable down to 10^{-4} pc, where the density reaches more than 500 $M_\odot \mathrm{pc}^{-3}$.

The left lower panel of Figure 2 shows the rough estimate of the phase-space density given by $\rho/\langle v^2 \rangle^{1.5}$, where $\langle v^2 \rangle$ is the velocity dispersion. The slope is close to -2.25 for $r < 10^{-3}$ pc. Because of Liouville's theorem, this phase-space density cannot exceed the initial value at the time of decoupling, which is $\sim 10^{15}\, M_\odot\, \mathrm{pc}^{-3}\, (\mathrm{km\, s}^{-1})^{-3}$. Thus, the gravitational collapse of the cusp stops at the radius at which the phase-space density reaches this limit. This radius and density there are $r_\mathrm{c} \sim 10^{-5}$ pc and $\rho_\mathrm{c} \sim 2 \times 10^4\, M_\odot\, \mathrm{pc}^{-3}$, respectively. We, therefore, can safely conclude that the density profile of microhalos is

$$\rho(r) = \rho_\mathrm{c}(r/r_\mathrm{c})^{-1.5} \quad \text{for} \quad 10^{-3}\,\mathrm{pc} \geqslant r \geqslant r_\mathrm{c}, \qquad (1)$$

and $\rho(r) \sim \rho_\mathrm{c}$ for $r < r_\mathrm{c}$. This profile is consistent with the results of early studies of the collapse of self-gravitating gaseous spheres (Suto & Silk 1988) and recent high-resolution simulations of cold collapse (Nipoti et al. 2006) and warm dark matter (Colín et al. 2008).

The average density of these Earth-mass halos is affected by density fluctuations of larger scales. However, our simulations do not contain large-scale fluctuations. As seen in Figure 3, Press–Schechter (Press & Schechter 1974) theory predicts that the average formation epoch of microhalos is earlier than those of our simulation if we take into account larger scale fluctuations. Since the average density of a microhalo should be proportional to the cube of its formation redshift, most microhalos should have higher average density than those in our calculation. For simplicity, we use the profile of Equation (1) to estimate the chance of survival of these halos.

3.2. Tidal Cutoff and Encounters with Stars

The tidal cutoff radius of microhalo with the density profile of Equation (1) due to galactic tide is expressed as $r_\mathrm{max} = 0.082(R/10\,\mathrm{kpc})^{4/3}$ pc, where R is the distance from the galactic center, if we assume an isothermal halo with the rotation velocity of 220 km s^{-1}. We can see that these halos can easily survive at the distance 1 kpc, and even at the distance 0.1 kpc, the central 10^{-4} pc of the halo would still survive.

Can encounters with stars destroy the internal cusps of microhalos (Berezinsky et al. 2003, 2006; Angus & Zhao 2007; Goerdt et al. 2007; Zhao et al. 2007; Green & Goodwin 2007; Schneider et al. 2010)? Since the surface number density of disk stars is about 100 pc^{-2} at the solar neighborhood, the closest distance a halo with the orbital period of the order of 100 Myr can approach to a star in the Hubble time is 10^{-2} pc.

Figure 4 shows the result of encounter with a $1\, M_\odot$ star moving at 200 km s^{-1}. We selected the most massive microhalo at $z = 31$ from the simulation of model A (the cutoff radius is two times virial value) and added velocities on each particle according to the impulsive approximation. Then, we simulated the evolution of the microhalo for 27 Myr after the encounter. We can see that the regions of radius $\sim 10^{-3}$ pc survive after encounters with the impact parameters of 0.02 pc. Theoretically, the cutoff radius due to encounter for the power-law cusp with slope -1.5 is given by $r \propto b^{8/11}$, where b is the impact parameter. Therefore, the complete disruption requires an encounter with $b = 5 \times 10^{-5}$ pc. Such close encounters are expected only at the very central regions of the galaxy (20 pc or less from the center).

If we extrapolate the subhalo mass function $dn/dm \propto m^{-2}$ (Berezinsky et al. 2003) to the mass of microhalos, the number of microhalos in our Galaxy is $\sim 5 \times 10^{16}$ (we assumed the mass function $dn/dm \sim 5 \times 10^{10}\, m^{-2}$). The number density

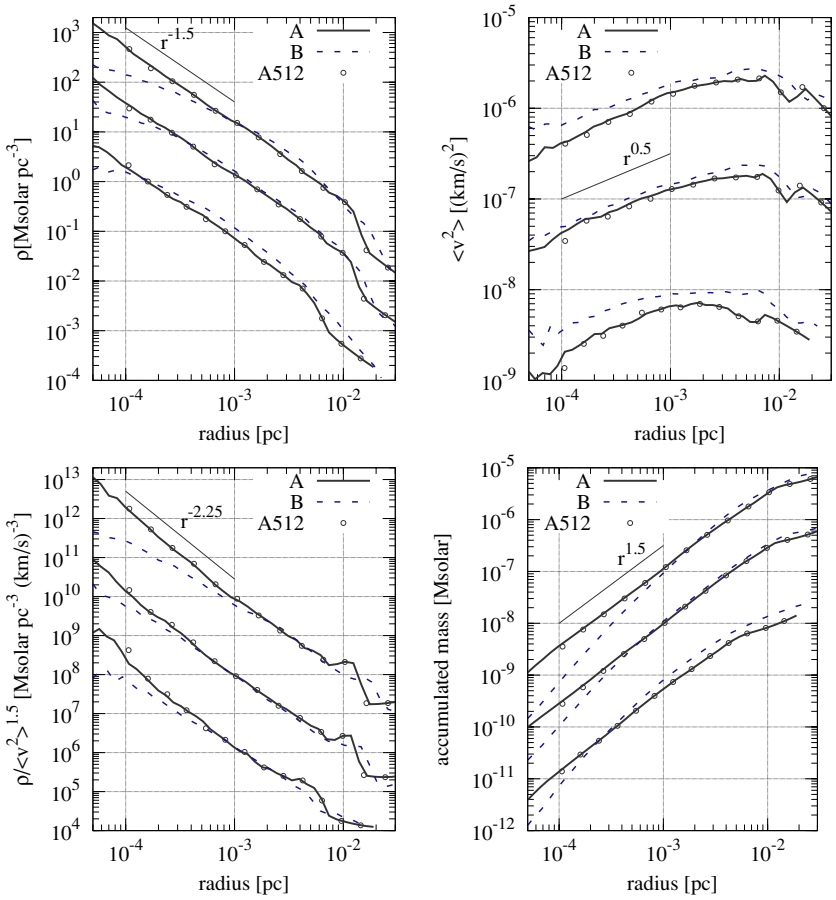

Figure 2. Radial profiles of three different microhalos of models A (black) and B (blue) at $z = 31$. Four panels show the density, velocity dispersion, phase-space density, and accumulated mass. Circles show profiles of a low-resolution simulation (A512: 512^3 particles, 1.0×10^{-4} pc softening length). Two out of three profiles (middle and bottom) are vertically shifted downward by 1 and 2 dex. In the panel of phase-space density profiles, the two profiles (middle and bottom) are shifted by 2 and 4 dex.

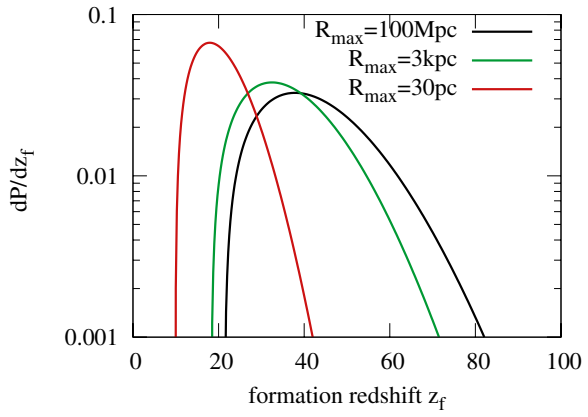

Figure 3. Differential probability distribution of the microhalo formation redshift predicted by Press–Schechter theory. The longest wavelength corresponds to 100 Mpc (black), 3 kpc (green), and 30 pc (red). These values correspond to the box length of the simulations by Diemand et al. (2005; 3 kpc) and this work (30 pc).

of the microhalos near the solar neighborhood is $\sim 500\,\mathrm{pc}^{-3}$, if the distribution of the microhalos is the same as that of the background dark matter. This extrapolation is justified by the fact that the microhalos survive under tides from our Galaxy. Note that the above estimate takes into account the effect of merging between small halos and accretion to somewhat larger halo since we extrapolated the mass function obtained by *N*-body simulation.

3.3. The Gamma-ray Luminosity of a Microhalo

The gamma-ray flux of a microhalo is given by

$$F_\gamma \sim \frac{N_\gamma \langle \sigma v \rangle}{2m_\chi^2} \frac{1}{4\pi d^2} \int_0^{r_{\max}} \rho^2 dV \tag{2}$$

$$\sim \frac{N_\gamma \langle \sigma v \rangle}{2m_\chi^2} d^{-2} \ln(r_{\max}/r_c) \rho_c^2 r_c^3, \tag{3}$$

$$\sim 9.2 \times 10^{-12} \frac{N_\gamma}{30} \frac{\langle \sigma v \rangle}{3 \times 10^{-26}\,\mathrm{cm^3\,s^{-1}}} \times \left(\frac{m_\chi}{100\,\mathrm{GeV}}\right)^{-2} \left(\frac{0.2\,\mathrm{pc}}{d}\right)^2 \tag{4}$$

$$\left(\frac{\rho_c}{2 \times 10^4\, M_\odot\,\mathrm{pc}^{-3}}\right)^2 \left(\frac{r_c}{10^{-5}\,\mathrm{pc}}\right)^3 \times \left(4.61 + \ln \frac{r_{\max}/10^{-3}\,\mathrm{pc}}{r_c/10^{-5}\,\mathrm{pc}}\right) \quad \mathrm{photons\,cm^{-2}\,s^{-1}},$$

where N_γ is the number of emitted photon per annihilation, m_χ is the mass of dark matter particle, $\langle \sigma v \rangle$ is the interaction cross section of dark matter, and $r_{\max}$ is the outer cutoff radius of a

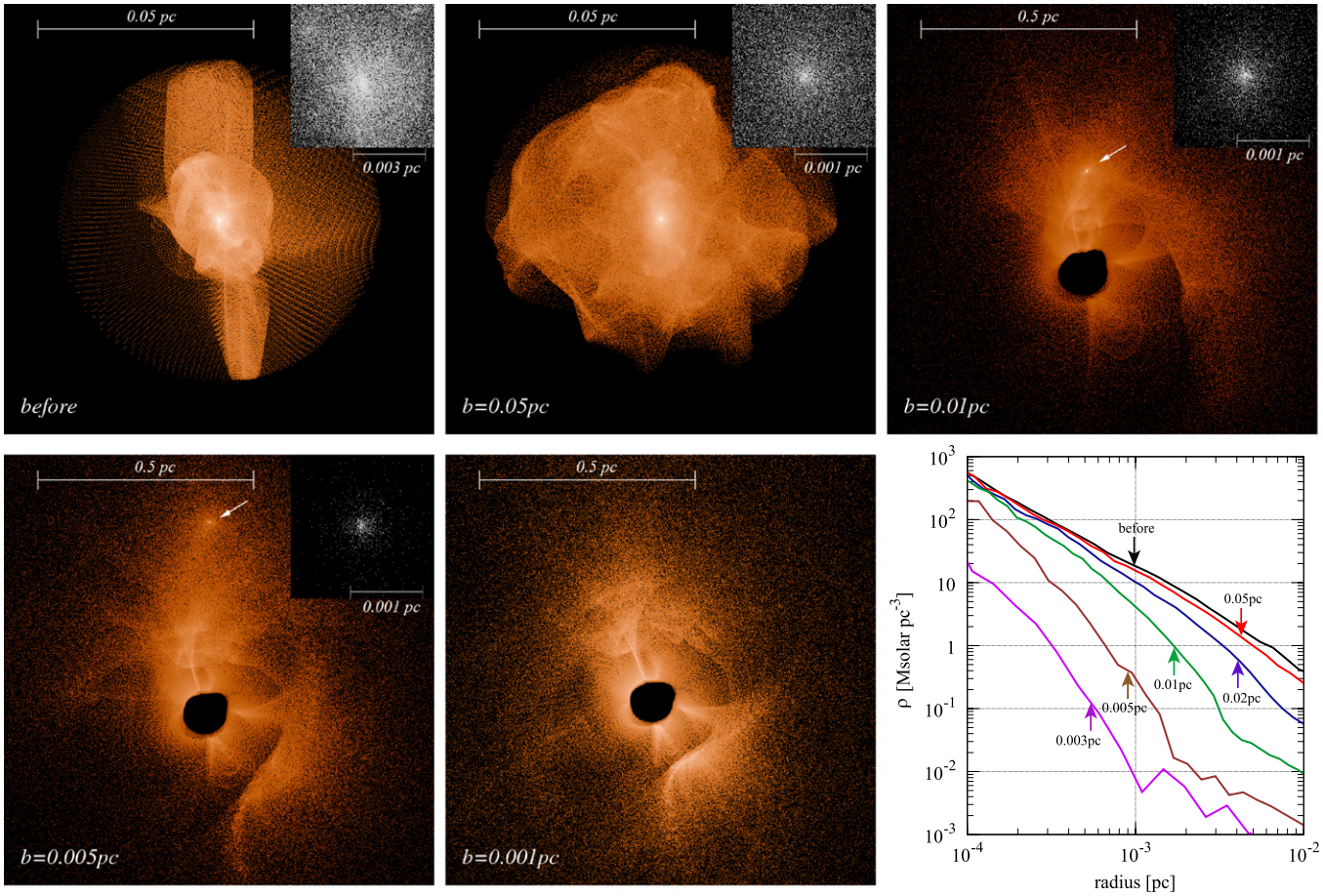

Figure 4. Snapshots and radial density profiles after encounters with stars. Panel (a) (top left) shows the snapshot of a halo in model A at $z = 31$. Only particles within the radius of 0.037 pc from the center of the halo are shown. Panels (b) (top middle), (c) (top right), (d) (bottom left), and (e) (bottom middle) show the distribution of particles at 27 Myr after the encounter with a solar-mass star with the impact parameters 5×10^{-2} pc, 1×10^{-2} pc, 5×10^{-3} pc, and 1×10^{-3} pc. The black regions in the center are caused by the initial outer cutoff of the particle distribution and are not real. The upper right box in each panel shows the central region of the microhalo. The central regions are located at the center (Panels (a) and (b)), and the positions indicated by arrows (Panels (c) and (d)). In panel (e), the central region is destroyed completely. Panel (f) (bottom right) shows the density profiles after the encounter.

microhalo at which the slope of the density becomes steeper than -1.5.

Mass loss due to the galactic tide or encounters with stars changes $r_{\rm max}$ of microhalos, but does not affect $\rho_{\rm c}$ or $r_{\rm c}$ except in the cases of extremely close encounters, as we can see in Figure 3. Therefore, they have a relatively minor effect on the gamma-ray luminosity. After 99% of the mass is lost from a microhalo, it still retains nearly 50% of the luminosity. Thus, we can assume that the tidal stripping has practically no effect on the gamma-ray luminosity of our Earth-mass halos. These results support the predictions of early analytical studies (Berezinsky et al. 2008).

Here, we consider how the gamma-ray flux of the microhalo depends on its formation epoch. The average density of a halo $\rho_{\rm ave}$ reflects the cosmic density at its formation time (Bullock et al. 2001). Since the cosmic density is proportional to $(1+z_{\rm f})^3$, $\rho_{\rm ave} \propto (\frac{1+z_{\rm f}}{1+z_0})^3$, where $z_{\rm f}$ and z_0 are the formation redshift and the typical formation redshift of microhalos in our simulations, respectively. From the conservation of the mass, we can derive $r_{\rm max} \propto \rho_{\rm ave}^{-1/3}$. We can rewrite $\rho_c^2 r_c^3$ in Equation (4) as $\rho_{\rm ave}^2 r_{\rm max}^3$ using Equation (1). Therefore,

$$F_\gamma(z_{\rm f}) \sim \left(\frac{1+z_{\rm f}}{1+z_0}\right)^3 F_\gamma. \quad (5)$$

Here, we drop the dependency of the formation redshift in the logarithmic term in Equation (4), since it is rather weak ($r_c \propto r_{\rm max}^{-1/3}$).

The average boost factor due to the formation epoch is determined as

$$\int \frac{dP(z_{\rm f})}{dz_{\rm f}} \frac{F_\gamma(z_{\rm f})}{F_\gamma(40)} dz_{\rm f}, \quad (6)$$

where $P(z_{\rm f})$ is the distribution function of the formation epoch. For the Press–Schechter function in Figure 3, its value is $\sim$1.6. We apply this boost factor to estimate the gamma-ray luminosity.

4. DISCUSSIONS AND SUMMARY

4.1. Gamma-ray Signal from Microhalos

There are many works on whether or not subhalos and microhalos can be observed via annihilation gamma ray (e.g., Oda et al. 2005; Koushiappas 2006; Ando et al. 2008; Lee et al. 2009; Kamionkowski et al. 2010; Schneider et al. 2010). We made the all-sky map of the gamma-ray annihilation signal in our Galaxy based on the new profile of the microhalo. The observer locates at 8.5 kpc from the center of the halo along its long axis. We consider the emissions from microhalos

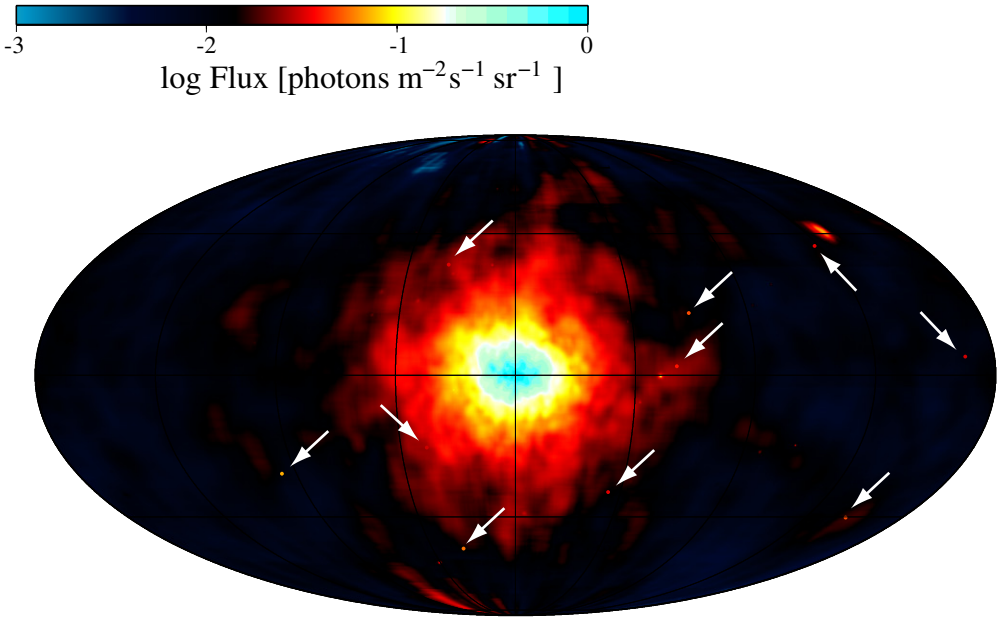

Figure 5. All-sky map of the gamma-ray annihilation signal of our Galaxy. Pointlike sources indicated by arrows show the contributions from microhalos less than 1 pc from the observer and with flux larger than 0.03 photons m^{-2} s^{-1} sr^{-1}. Here, we assume that the number of photons per annihilation is $N_\gamma = 30$, the interaction cross section of dark matter is $\langle \sigma v \rangle = 3.0 \times 10^{-26}$ cm^3 s^{-1}, and the mass of dark matter particle is $m_\chi = 100$ GeV. The flux of the integrated emission of microhalos in the galactic center is 1.40 photons m^{-2} s^{-1} sr^{-1}. The flux of the most brightest microhalo is 0.069 photons m^{-2} s^{-1} sr^{-1}. The flux needed for a 10σ detection for *Fermi* is $\sim 0.4 \times 10^{-6}$ photons cm^{-2} s^{-1} for low Galactic latitude and is $\sim 0.1 \times 10^{-6}$ photons cm^{-2} s^{-1} for high Galactic latitude (Abdo et al. 2009a). The angular resolution of *Fermi* is about 0.1 deg for energies above 1 GeV.

only. We assume that the spatial distribution of microhalos follows the mass distribution of a galaxy-sized LCDM halo selected from our previous simulation (Ishiyama et al. 2009a). Thus, our all-sky map naturally includes all subhalos with the mass larger than the numerical limit ($\sim 10^8\ M_\odot$). In addition, destruction due to encounters with stars is taken into account. We assumed an exponential disk with the surface density, $\Sigma(r) \sim 1000 \exp(-r/3\,\mathrm{kpc})\,\mathrm{pc}^{-2}$, where r is the distance from the galactic center. From the position of an ensemble of microhalos, the impact parameter b of encounters with stars is calculated. Then, we use the cutoff radius $r_{\rm cut} = 0.017 b^{8/11}$pc and reduce the gamma-ray luminosity.

In order to include the luminosities of nearby microhalos, we placed randomly 2000 microhalos less than 1 pc from the observer. The distribution of formation redshift and the gamma-ray flux of microhalos are given by Figure 3 and Equation (5).

Figure 5 shows the all-sky map. Many nearby microhalos are observed as pointlike sources, since their angular size is around $1'$. Therefore, the nearby microhalos are promising sources of the gamma-ray signal of the annihilation of dark matter particles. Their distance is around 10^4 AU and velocity is of the order of 200 km s^{-1}. The proper motion is as large as 0.2 deg yr^{-1}. They might be too dim to be observed by *Fermi*. The Sommerfeld effect could boost the interaction cross section of dark matter and enhance by orders of magnitude the gamma-ray luminosity (Kuhlen et al. 2009). These microhalos might be good targets of the next generation Cherenkov telescope, such as the Cherenkov Telescope Array.[3]

Bright microhalos enhance luminosities of all subhalos (including known Milky Way satellite) since subhalos contain a number of microhalos. The brightest gamma-ray source is the integrated emission of microhalos in the galactic center, but it is much more extended compared to the result of previous studies (Springel et al. 2008). These sources may also be good targets for observation. However, baryons would have significant effect on the distribution of dark matter at the center of the galaxy. If baryons disrupt the central cusp of the main halo (Mashchenko et al. 2006, 2008; Governato et al. 2010), the gamma-ray flux from the galactic center might be much smaller. Observational data suggest that dwarf galaxies have constant density cores (e.g., Gentile et al. 2004).

4.2. Perturbations on Millisecond Pulsars

Pulsar timing measurements might be used to detect microhalos. Since many of known millisecond pulsars (MSPs) are in the direction of the galactic center, the number density of microhalos around MSPs is higher than that of solar neighborhood.

Here, we estimate the residual of the time of arrival of an MSP due to the gravitational attraction from its nearest neighbor, following Seto & Cooray (2007). The residual due to the constant acceleration a in the period of t is given by

$$\Delta T = \frac{at^2}{2c}, \tag{7}$$

where c is the speed of light and a is given by

$$a = -\frac{GM}{R^2}, \tag{8}$$

where G, M, and R are the gravitational constant, the mass of the microhalo, and the distance between the microhalo and the MSP, respectively. So we have

$$\Delta T = 10.8 \left(\frac{R}{2 \times 10^4\ \mathrm{AU}}\right)^{-2} \left(\frac{M}{10^{-6}\ M_\odot}\right) \left(\frac{t}{20\ \mathrm{yr}}\right)^2 \ \mathrm{ns}. \tag{9}$$

If we assume that a microhalo lost 90% of mass by encounters with stars, the residual is about $\sim$2 ns in 20 years. The change of

[3] http://www.cta-observatory.org/

the distance in 10 years is around 400 AU. Since the change in the acceleration is proportional to the third power of the distance, one in ten MSPs would show the change in the acceleration 10 times larger than that of a typical MSP, which should be detectable with Parkes Pulsar Timing Array (Manchester 2008) after modest improvement in the timing accuracy.

Note that the mass loss of two weak encounters can be larger than that of a strong encounter (Angus & Zhao 2007). For simplicity, we used the mass loss due to a strong encounter as estimated in Section 3.2. However, the mass loss of microhalos in the opposite direction to the galactic center is less than that near Sun. MSPs in this direction should show larger timing residuals.

4.3. Summary

We found that Earth-mass microhalos have steep central density cusps. Their central regions are not disrupted by tidal forces from the parent galaxies or stars, and they survive to the present time. Our result is different from the recent claims that small-scale structure have a negligible impact on dark matter detectability (Springel et al. 2008). They considerably underestimate annihilation signals because they assumed that the density profile for the smallest microhalos was shallower than what we found with high-resolution simulations.

We are grateful to Veniamin Berezinsky for helpful discussions. Numerical computations were carried out on Cray XT4 at Center for Computational Astrophysics, CfCA, of National Astronomical Observatory of Japan. T.I. is financially supported by Research Fellowship of the Japan Society for the Promotion of Science (JSPS) for Young Scientists. This research is partially supported by the Special Coordination Fund for Promoting Science and Technology (GRAPE-DR project), Ministry of Education, Culture, Sports, Science and Technology, Japan.

REFERENCES

Abdo, A. A., et al. 2009a, ApJS, 183, 46
Abdo, A. A., et al. 2009b, Phys. Rev. Lett., 102, 181101
Adriani, O., et al. 2009, Nature, 458, 607
Ando, S., Kamionkowski, M., Lee, S. K., & Koushiappas, S. M. 2008, Phys. Rev. D, 78, 101301
Angus, G. W., & Zhao, H. 2007, MNRAS, 375, 1146
Berezinsky, V., Dokuchaev, V., & Eroshenko, Y. 2003, Phys. Rev. D, 68, 103003
Berezinsky, V., Dokuchaev, V., & Eroshenko, Y. 2006, Phys. Rev. D, 73, 063504
Berezinsky, V., Dokuchaev, V., & Eroshenko, Y. 2008, Phys. Rev. D, 77, 083519
Bode, P., Ostriker, J. P., & Turok, N. 2001, ApJ, 556, 93
Bullock, J. S., Kolatt, T. S., Sigad, Y., Somerville, R. S., Kravtsov, A. V., Klypin, A. A., Primack, J. R., & Dekel, A. 2001, MNRAS, 321, 559
Chang, J., et al. 2008, Nature, 456, 362
Colín, P., Valenzuela, O., & Avila-Reese, V. 2008, ApJ, 673, 203
Diemand, J., Moore, B., & Stadel, J. 2005, Nature, 433, 389
Fukushige, T., Kawai, A., & Makino, J. 2004, ApJ, 606, 625
Fukushige, T., & Makino, J. 1997, ApJ, 477, L9
Gao, L., & Theuns, T. 2007, Science, 317, 1527
Gentile, G., Salucci, P., Klein, U., Vergani, D., & Kalberla, P. 2004, MNRAS, 351, 903
Goerdt, T., Gnedin, O. Y., Moore, B., Diemand, J., & Stadel, J. 2007, MNRAS, 375, 191
Governato, F., et al. 2010, Nature, 463, 203
Green, A. M., & Goodwin, S. P. 2007, MNRAS, 375, 1111
Green, A. M., Hofmann, S., & Schwarz, D. J. 2004, MNRAS, 353, L23
Hofmann, S., Schwarz, D. J., & Stöcker, H. 2001, Phys. Rev. D, 64, 083507
Ishiyama, T., Fukushige, T., & Makino, J. 2009a, PASJ, 61, 1319
Ishiyama, T., Fukushige, T., & Makino, J. 2009b, ApJ, 696, 2115
Kamionkowski, M., Koushiappas, S. M., & Kuhlen, M. 2010, Phys. Rev. D, 81, 043532
Komatsu, E., et al. 2009, ApJS, 180, 330
Koushiappas, S. M. 2006, Phys. Rev. Lett., 97, 191301
Kuhlen, M., Madau, P., & Silk, J. 2009, Science, 325, 970
Lee, S. K., Ando, S., & Kamionkowski, M. 2009, J. Cosmol. Astropart. Phys., JCAP07(2009)007
Loeb, A., & Zaldarriaga, M. 2005, Phys. Rev. D, 71, 103520
Manchester, R. N. 2008, in AIP Conf. Ser. 983, 40 Years of Pulsars: Millisecond Pulsars, Magnetars and More, ed. C. Bassa et al. (Melville, NY: AIP), 584
Mashchenko, S., Couchman, H. M. P., & Wadsley, J. 2006, Nature, 442, 539
Mashchenko, S., Wadsley, J., & Couchman, H. M. P. 2008, Science, 319, 174
Moore, B., Quinn, T., Governato, F., Stadel, J., & Lake, G. 1999, MNRAS, 310, 1147
Navarro, J. F., Frenk, C. S., & White, S. D. M. 1996, ApJ, 462, 563
Navarro, J. F., et al. 2010, MNRAS, 402, 21
Nipoti, C., Londrillo, P., & Ciotti, L. 2006, MNRAS, 370, 681
Oda, T., Totani, T., & Nagashima, M. 2005, ApJ, 633, L65
Press, W. H., & Schechter, P. 1974, ApJ, 187, 425
Prunet, S., Pichon, C., Aubert, D., Pogosyan, D., Teyssier, R., & Gottloeber, S. 2008, ApJS, 178, 179
Schneider, A., Krauss, L. M., & Moore, B. 2010, Phys. Rev. D, 82, 063525
Seto, N., & Cooray, A. 2007, ApJ, 659, L33
Spergel, D. N., et al. 2003, ApJS, 148, 175
Spergel, D. N., et al. 2007, ApJS, 170, 377
Springel, V., et al. 2008, Nature, 456, 73
Stadel, J., Potter, D., Moore, B., Diemand, J., Madau, P., Zemp, M., Kuhlen, M., & Quilis, V. 2009, MNRAS, 398, L21
Suto, Y., & Silk, J. 1988, ApJ, 326, 527
Torii, S., et al. 2008, arXiv:0809.0760
Zhao, H., Hooper, D., Angus, G. W., Taylor, J. E., & Silk, J. 2007, ApJ, 654, 697
Zybin, K. P., Vysotsky, M. I., & Gurevich, A. V. 1999, Phys. Lett. A, 260, 262